RESEARCH ARTICLE

Engineering Reports

WILEY

Computational fluid dynamics of coronary arteries with implanted stents: Effects of Newtonian and non-Newtonian blood flows

Fatemeh Ahadi[1] | **Mojtaba Biglari[1]** | **Mohammad Azadi[1]** | **Mahdi Bodaghi[2]**

[1]Faculty of Mechanical Engineering, Semnan University, Semnan, Iran

[2]Department of Engineering, School of Science and Technology, Nottingham Trent University, Nottingham, UK

Correspondence
Mohammad Azadi, Faculty of Mechanical Engineering, Semnan University, Semnan, Iran.
Email: m_azadi@semnan.ac.ir

Abstract

This study introduces and compares computational fluid dynamics of Newtonian and non-Newtonian blood flows in coronary arteries, with and without considering stents. Three blood flow models, including Newtonian, Carreau, and non-Newtonian power-law models, were simulated to investigate their effect, and the solution algorithm includes drawing the geometry, creating the desired mesh, and then simulating Newtonian and non-Newtonian blood flow different models and comparing them with each other, is presented in the article. A Newtonian fluid model has been commonly used in the simulation of blood flow, whereas blood has non-Newtonian properties due to the nature of a solution containing suspended particles. The goal of this research is to investigate the differences between the models built with Newtonian and non-Newtonian fluid assumptions. In addition, a stent was designed and the effect of the stent on blood flow parameters was investigated for all three flow models, including Newtonian, Carreau, and non-Newtonian power-law models. Stents are medical devices that can be placed in arteries to open up blood flow in a blocked vessel. Stents can affect the wall shear stress. Knowing the slight deformation of the shear stress makes the importance of stent implantation and also helps to optimize the design of the intravascular stent, which can affect the occlusion of the vessels. The distribution of the velocity, pressure, and wall shear stress in all blood flow models with and without considering the effect of stents have been investigated and finally compared. Therefore, in general, the innovation of this article is to find the effect of implanted stents on blood flow parameters with different blood flow models, both Newtonian and non-Newtonian. A comparison of Newtonian and non-Newtonian flows showed that in the case of the Carreau non-Newtonian model, the wall shear stress was higher. In addition, in the results of the geometric model with a stent effect compared to the geometric model without a stent effect, it is evident that there was a higher velocity and wall shear stress.

KEYWORDS

blood flow, computational fluid dynamics, Newtonian model, non-Newtonian model, stent

1 | INTRODUCTION

The study of blood flow is called hemodynamics and it has been one of the engrossing physiological topics in recent years. Blood contains various cells including red blood cells, white blood cells, and platelets in plasma. Hemodynamics explains the physical laws that govern the flow of blood in the blood vessels. Blood flow ensures the transportation of nutrients, hormones, metabolic waste products, oxygen, and carbon dioxide throughout the body to maintain cell-level metabolism, the regulation of the pH, osmotic pressure, and temperature of the whole body, and the protection from microbial and mechanical harm. With the development of computational biomechanics, some researchers[1–5] have performed numerical simulations of blood flow. Blood has been considered a Newtonian fluid for decades, but recent experiments have shown that blood has pronounced viscoelastic behavior.[6] In general, blood is really a non-Newtonian fluid. Therefore, numerical simulation is suggested as an important and useful tool for understanding blood flow behavior.[7,8] Blood is a complex fluid, including proteins and living cells floating in plasma. Therefore, it is important to have knowledge and information about blood in the arteries to recognize and prevent vascular diseases.[9] The red blood cells in the blood change the properties of the blood fluid and affect its behavior. Moreover, on the other hand, clogging in the vessels can cause a reduction and slowdown of the blood flow; in addition, the wall shear stress can cause clogging of the vessels, so studying the hemodynamic factors related to the vessel and blood to understand the physiology of diseases arterial is important.[10] In 1997, a large number of empirical and numerical studies were reported on flows and stents,[11] and many resources were used as different mathematical models for analysis.[8,12]

Toghraie et al.[13] performed a numerical study of smooth arterial blood flow, where they introduced the blood as a simulated non-Newtonian fluid. Furthermore, in another study,[14] these researchers compared the behavior of Newtonian and non-Newtonian blood flows. They have published applications of their findings in several therapies that effectively alter blood behavior. Moreover, other researchers[15–18] presented applications of experimental and numerical methods that can be used in medical treatment. Chen and Lu[19] considered blood as a Carreau-Yasuda fluid and studied the wall shear stress. Perktold et al.,[20] considering blood as a Newtonian fluid, compared the velocity profile and the wall shear stress distribution with the experimental results of Ku and Giddens.[21] In addition, Joe and Berger[22] assumed that the flow in the carotid bifurcation was Newtonian and simulated steady and unsteady flows.

In addition to examining blood flow models, one of the other important topics in this field of study is vascular occlusion.[23–26] There are several ways to unblock arteries, one of which is stenting. Stents are cylindrical scaffolds to unblock arteries.[27,28] Today, the use of stents for coronary vessels has increased greatly.[29] Therefore, it is very important to analyze the behavior of stents mechanically.[30] The mechanical analysis of the behavior in stents means investigating the behavior of stents under different conditions of loading, temperature, etc., using solid and finite element mechanics theory. In this regard, the mechanical analysis of the behavior in stents includes the examination of changes in the length, diameter, and shape of the stent in response to loading and temperature, as well as the examination of changes in stress and strain in the intended stent.[31,32] The results of studies on the structure of stents showed that each stent topology has its own structural and hemodynamic function.[33,34] In addition, optimized geometries for stents and their surfaces help to reduce thrombosis.[35]

In addition, the mechanical properties of arteries are very important for understanding the pathophysiology of cardiovascular diseases. In the investigation of vascular tissue, it is essential to analyze and compare various types of vascular models. According to the sources, vessels can be considered elastic, viscoelastic, or hyper-elastic, depending on the definition of each of these models, different results are obtained. Then, they can be compared with each other. Consequently, it can be noted that the mechanical structure of the artery walls and their properties determine the mechanical behavior of the artery.[10,23–26]

Based on the review of the open literature, it can be concluded that (1) blood has a non-Newtonian nature, but in many simulations, it has been considered Newtonian; (2) three blood models, Newtonian, non-Newtonian Carreau, and non-Newtonian power-law have been widely used models in the simulation of blood flows; (3) the non-uniform stress distribution was observed in the blood flow with the stent at the stenting site; and (4) in addition, the results illustrated that each stent topology had its own structural and hemodynamic performance.

Based on the review of the literature, it can be claimed that considering Newtonian flow for blood flow alone is not reliable. Therefore, in this study, two non-Newtonian Carreau and power-law models were used in the blood flow simulation along with a Newtonian model. Therefore, after verifying the simulation, all blood flow models were examined together with the same boundary conditions for a coronary vessel. In addition, based on previous studies, the investigation of these three blood flow models along with the stent effect has not been presented so far. Therefore, this research is presented to study three different blood flow models, before and after the effect of stenting. Therefore, the innovation of this

article is to find the effect of implanted stents on the fluid characteristics with different Newtonian and non-Newtonian blood flow models.

2 | RESEARCH METHODS

2.1 | Developed flow

If fluid with a uniform velocity profile enters the circular cross-section as shown in Figure 1, as soon as the fluid enters, then fluid viscosity effects cause the fluid to stick to the wall, which is referred to as the no-slip condition. The no-slip condition indicates that the fluid in the vicinity of a wall moves with a velocity equal to the velocity of the same wall. In this region, the fluid boundary layer is formed around the wall, in the boundary layer region, viscosity effects are important. As shown in Figure 1, the region at the inlet where the effects of viscosity and boundary layer do not cover the entire cross-section is called the entrance region, whose length is equal to the entrance length. In the entrance area, the fluid velocity profile changes gradually along the section. This change continues until the fluid reaches the end of the entrance region, after which the flow becomes fully developed.[36]

In this research, with an arterial diameter of 3 mm and a blood flow velocity of 0.105 m/s, the Reynolds number is in the laminar flow range (Re < 2300), and the inlet length is considered long enough to fully develop the flow according to Equation (1)[36];

$$\frac{L_e}{D} = 0.06 \, Re \qquad \text{For laminar flow,} \tag{1}$$

$$\frac{L_e}{D} = 4.4 \, (Re)^{1/6} \qquad \text{For turbulent flow,} \tag{2}$$

$$Re = \frac{\rho \, V \, D}{\mu}, \tag{3}$$

$$\begin{cases} Re \leq 2300; & \text{Laminar,} \\ 2300 \leq Re \leq 4000; & \text{Transition,} \\ Re \geq 4000; & \text{Turbulent.} \end{cases} \tag{4}$$

2.2 | Design

In the simulation of this research, the objective was to compare the results of Newtonian and non-Newtonian models of blood flow in a coronary artery.

To choose the diameter range of coronary arteries according to the classification of studies presented in Table A1 of References 37–44 in Appendix A, a diameter of 3 mm was chosen for this research.
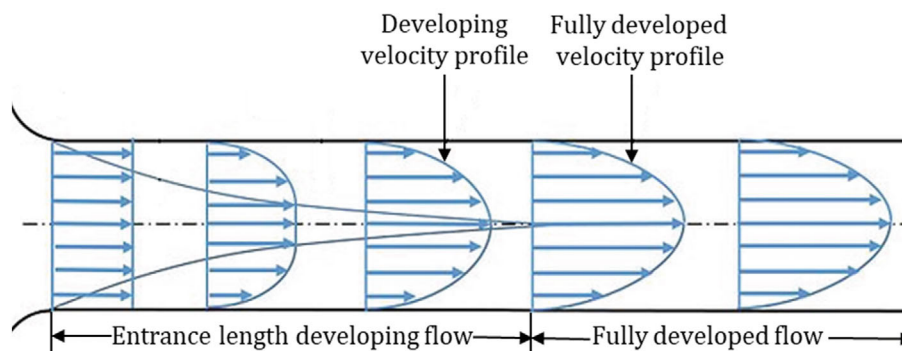

FIGURE 1 The velocity profile for the laminar flow.

T A B L E 1 Geometry parameters for blood flow and stent.

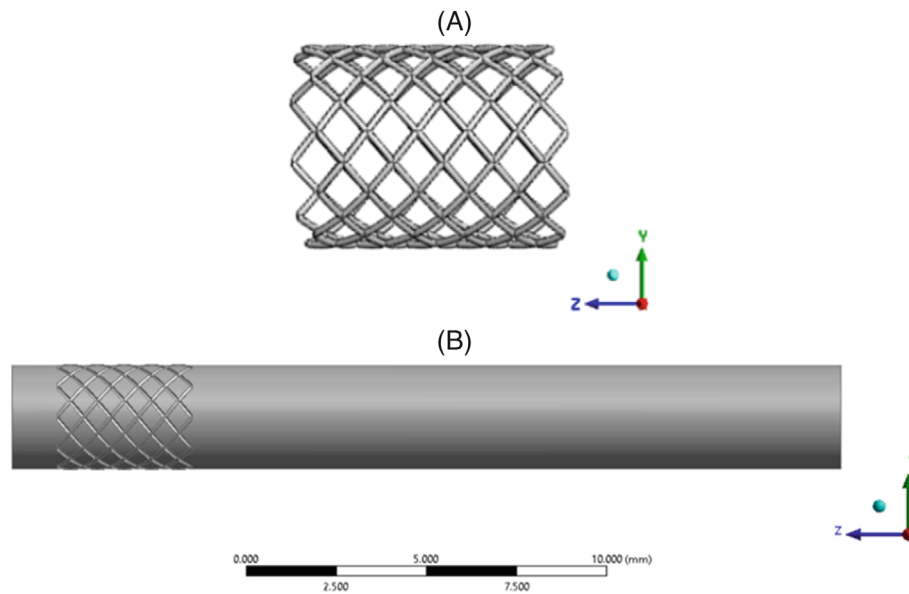| Geometry parameters for blood flow	Dimensions (mm)	Geometric parameters for stent	Dimensions (mm)
Diameter of the circle	3	Internal diameter	2.95
		Outer diameter	3.05
Length of the circle	23	Stent thickness	0.10
		Stent length	3.75

F I G U R E 2 The modeled components: (A) stent and (B) blood flow with stent effect.

In Table 1, the geometric parameters of this problem are given. The modeled stent geometry for the problem is also depicted in Figure 2 (where the geometry was similar to the reference[45]). The designed stent was drawn in solid-work. In Table 1, the geometric parameters of this problem, including inner diameter, outer diameter, strut thickness, and stent length, are given. Figure 2 also shows the geometric model of the image of the stent effect on the blood flow model.

2.3 | Mesh generation and modeling

To create a regular mesh, a square was drawn in the middle of the blood flow geometry to create a regular mesh. For the independence of the mesh and to find the minimum number of mesh elements with which accurate calculations can be made, several different sizes of meshing were investigated to discretize the problem. In Figure 3, the convergence diagram of the mesh is also given. As it is clear, Mesh 1 was the coarsest size, and the results of Mesh 4 and Mesh 5 were close to each other; The velocity difference percentage for two Mesh series 4 and 5 was 0.05%, therefore Mesh series 4 was chosen to continue the solution. Examining the wall shear stress also illustrated the same issue. The meshing process for the geometry considering the stent, requires finer meshing. This meshing was created due to the fineness and accuracy of the meshing in the Fluent with Fluent Meshing software. Different meshing was investigated in terms of geometry to achieve mesh independence. The mesh convergence diagram is shown in Figure 3, which depicts the maximum velocity and maximum wall shear stress for the number of elements. Statistics indicated that the results of Mesh 3 and Mesh 4 were close to each other. The velocity difference percentage for two Meshes Series 3 and 4 was 0.14%; therefore, Mesh 3 was chosen to continue the solution. Examining the wall shear stress also demonstrated the same issue. Meshing for blood flow without and with the stent is shown in Figure 4.
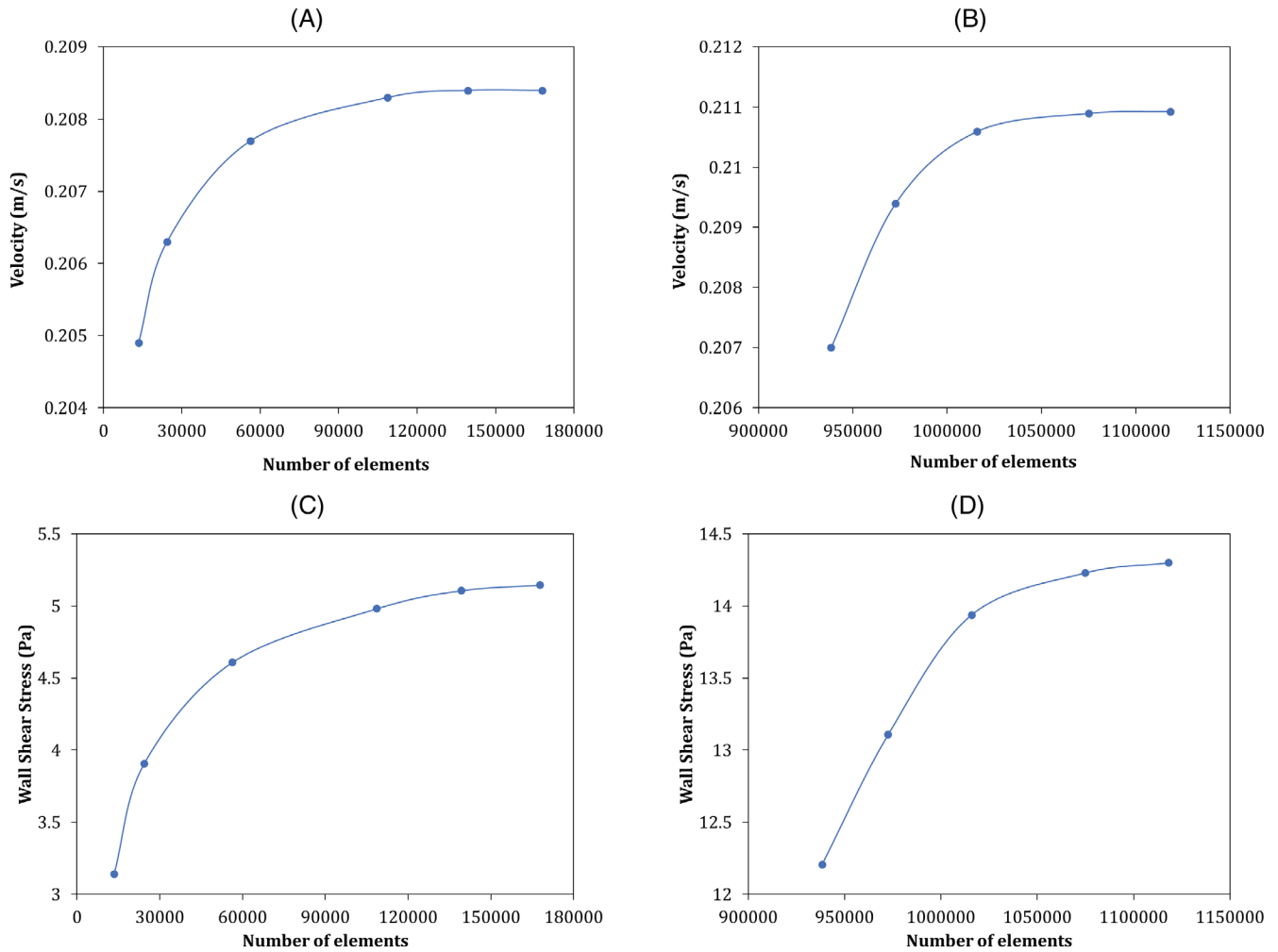
FIGURE 3 The mesh convergence diagram for (A) the velocity in the blood flow model, (B) the velocity in the blood flow model with stent effect, (C) the wall shear stress in the blood flow model, and (D) the wall shear stress in the blood flow model with stent effect.

In this research, the equations were solved by the SIMPLEC algorithm (semi-implicit method for pressure linked equations-consistent) and pressure-based solver under the mentioned boundary conditions. Moreover, the gravity of 9.81 (m/s^2) was also considered. In the inlet, the velocity was defined as 0.105 m/s,[46] at the outlet, the outlet pressure was defined, the wall condition was also considered in the blood flow wall, and the cross-section was considered symmetrical. During the solution process, the residuals by definition, all reached 10^{-6} and also converged. The flow was also considered incompressible, steady-state, and laminar.

2.4 | Mathematical model

In this research, three blood rheology models were investigated, including a Newtonian model and two non-Newtonian models. Non-Newtonian models include two models, Carreau and non-Newtonian power-law.

The solution algorithm for Newtonian flow and two non-Newtonian flow models, in Ansys Fluent software, is shown in Figure 5.

Viscosity for the Newtonian blood flow model was a constant number ($\mu = 0.0035$ (kg/m.s)).[47,48]

Based on the Carreau model, domains with low shear rates and complex shear-thinning rheology can be modeled perfectly[47];

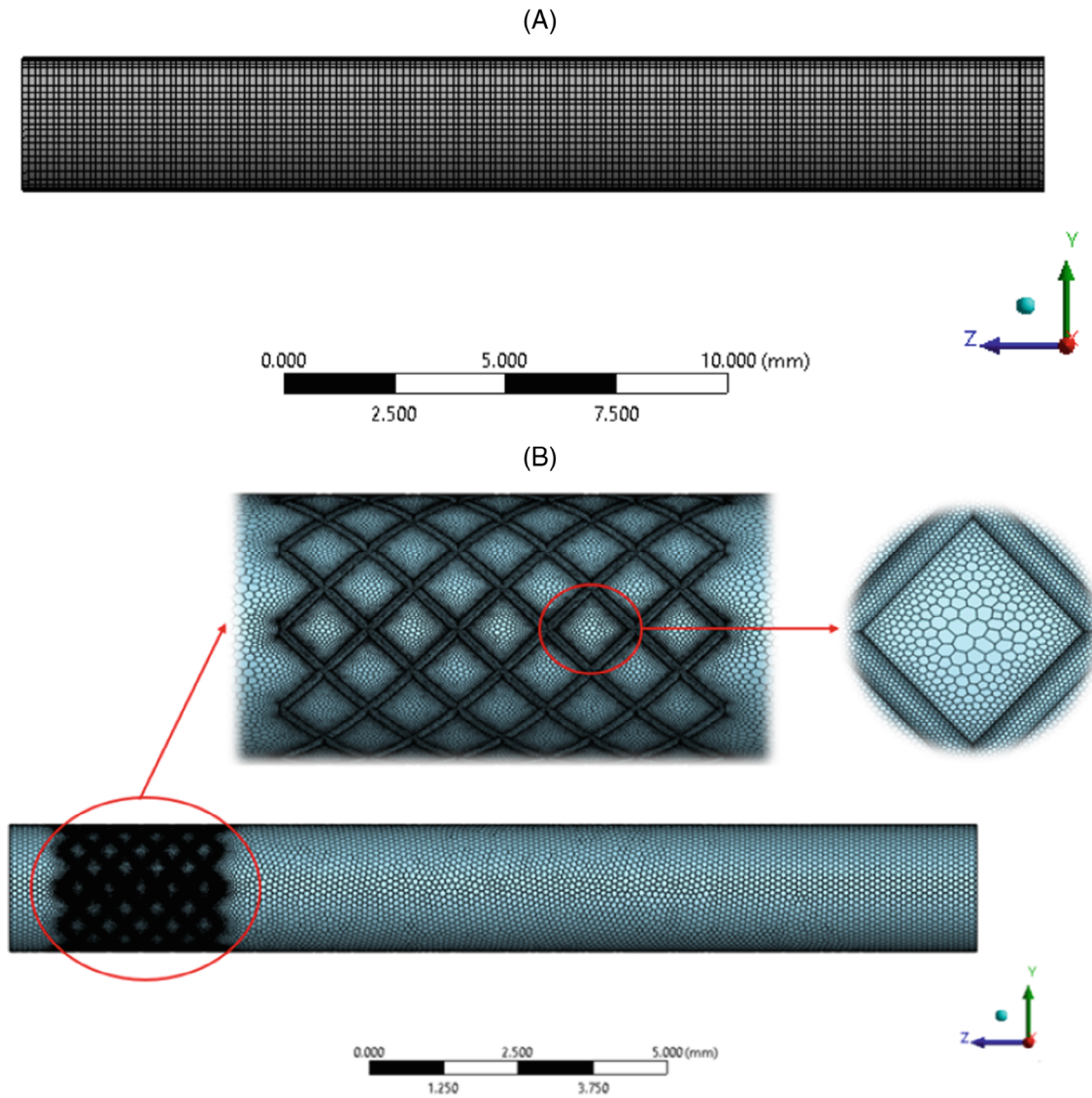$$\tau_{ij} = 2\mu(\dot{\gamma})d_{ij}, \tag{5}$$

(A)

(B)

FIGURE 4   Meshing (A) blood flow model and (B) blood flow model with stent effect.

Such models are called generalized Newtonian models, and contrary to Newtonian models, the viscosity is not constant but a function of shear rate[47];

$$\dot{\gamma} = \sqrt{2d_{ij}d_{ij}}, \tag{6}$$

Carreau's law is one of the most commonly rheological models of blood, which is expressed as the following equation[47,49,50];

$$\mu = \mu_\infty + (\mu_0 - \mu_\infty)\left(1 + K^2\dot{\gamma}^2\right)^{\frac{n-1}{2}}. \tag{7}$$

Non-Newtonian power-law viscosity is calculated according to the following equation[47,48,51];

$$\mu = k\dot{\gamma}^{n-1}e^{T_0/T} \tag{8}$$

To define the non-Newtonian power-law model in the software, it is necessary to determine the maximum and minimum viscosity, which is expressed as Equation (9)[47,48,51];

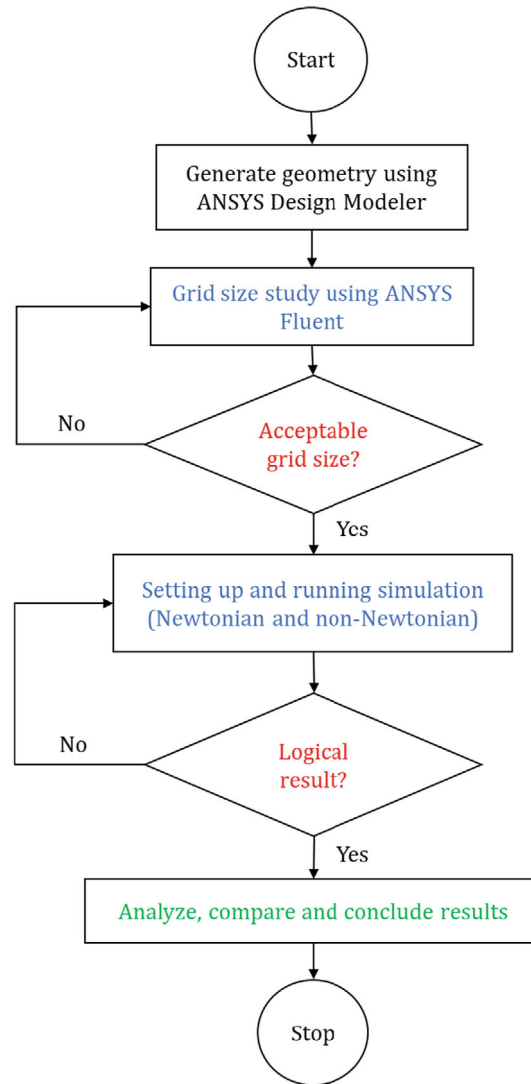$$\mu_{min} < \mu = k\dot{\gamma}^{n-1}e^{T_0/T} < \mu_{max}. \tag{9}$$

FIGURE 5   The algorithm of the solution process.

2.5 | Material properties

In this research, a FLUENT solver was used for simulating Newtonian and non-Newtonian flows. To solve this problem, FLUENT needs data to implement the solution. The required data includes the solution model or method, material properties, boundary conditions for a given problem, and the initial conditions required for the solution process, which are defined in the continuation of all parameters. At first, in the problem-solving phase, the model should be validated with other models to be reliable. In this study, the blood circulation velocity was considered to be 0.105 m/s.[46] Below are the details of the parameters of different Newtonian and non-Newtonian models of blood. In Table 2, the problem inputs for blood flow are given.

The input parameters for Newtonian and non-Newtonian flows including Carreau and non-Newtonian power-law in the equations of the mathematical model section are given in Table 2.

3 | RESULTS AND DISCUSSION

In this research, Newtonian and non-Newtonian models of blood flow with and without considering the effect of stents were investigated, as mentioned. The results were obtained using simulation in Ansys Fluent software. In the following part, first, the validation results and then the results of three flow models without and considering the stent effect are given.

TABLE 2 Input parameters for Newtonian and non-Newtonian flows.

Parameters	Values
Newtonian model[47,48]	
Density (kg/m³)	1060
Viscosity (kg/m.s)	0.0035
Carreau model[47,52]	
Density (kg/m³)	1060
Time constant (s)	3.3130
Index, n	0.3568
Zero shear viscosity (kg/m.s)	0.0560
Infinite shear viscosity (kg/m.s)	0.0035
Non-Newtonian power-law[47,48,51]	
Density (kg/m³)	1060
Consistency Index, k (kg.s^{n-2}/m)	0.2073
Power-law index, n	0.4851
Minimum viscosity limit, μ_{min} (kg/m.s)	0.0013
Maximum viscosity limit, μ_{max} (kg/m.s)	0.0035

TABLE 3 The validation of the Newtonian blood model at three different Reynolds numbers with Reference [53] and with the exact solution.

Parameters	Reynolds	Exact solution	Reference[53]	Newtonian Model	Relative error with exact solution (%)	Relative error with Reference[53] (%)
Velocity (m/s)	50	0.0330	0.0329	0.0328	0.61	0.30
	100	0.0660	0.0658	0.0655	0.76	0.46
	200	0.1320	0.1311	0.1307	0.98	0.31
Pressure drop per unit length (mPa/mm)	50	73.9200	73.9196	72.7310	1.61	1.61
	100	147.8400	147.8617	145.3016	1.72	1.73
	200	295.6800	295.7867	289.8630	1.97	2.00
Average wall shear stress (Pa)	50	0.0924	0.0923	0.0914	1.09	0.98
	100	0.1847	0.1848	0.1824	1.26	1.32
	200	0.3696	0.3696	0.3643	1.45	1.45

3.1 | Validation

As a first result, in this section, the validity of the simulation for intravascular blood flow is demonstrated. The desired geometry is modeled according to Reference 53, including a cylinder with a length of 0.1 m and a diameter of 0.005 m with the CFD results of that reference and also with the exact solution whose equations are given in Appendix B, based on the reference,[54] modeled and validated. In addition, the equations in the boundary conditions of the model were defined based on Reference 53, including the inlet velocity and outlet pressure ($P = 0$ Pa), considering the boundary conditions of non-slip in the wall and the rigid wall. In addition, the model used in this validation[53] was considered to be a three-dimensional, incompressible, laminar, and steady model. In addition, the blood flow was modeled as a Newtonian flow with a density of 1060 kg/m³ and a viscosity of 0.0035 Pa.s. The validation for velocity and pressure drop along the length and wall shear stress in three Reynolds of 50, 100, and 200 was done, which is reported in Table 3. As can be seen, all the errors were below 2%, and with the increase of the Reynolds number, the errors

TABLE 4 The validation of the non-Newtonian blood model with reference.[53]

Parameters	Reynolds	Reference[53]	Non-Newtonian Model	Relative error with Reference [53] (%)
Velocity (m/s)	50	0.1000	0.0996	0.40
	100	0.1650	0.1641	0.55
	200	0.2700	0.2680	0.74
Pressure drop per unit length (mPa/mm)	50	460.3055	454.4650	1.27
	100	619.5869	609.3480	1.65
	200	833.9804	817.0873	2.03
Average wall shear stress (Pa)	50	0.5753	0.5793	0.70
	100	0.7743	0.7639	1.34
	200	1.0422	1.0276	1.40

also increased. In addition, the highest percentage of errors was respectively for the pressure drop per unit length and then the shear stress of the wall and after that, it was the speed. As a result, it can be claimed that a proper simulation was performed in this research and the obtained results were confirmed and validated with the data available in the reference literature.[53] In Table 4, A validation for a non-Newtonian flow model has also been carried out. The flow was considered laminar and steady. In addition, blood flow was modeled as a non-Newtonian power-law ($k = 0.035$ Pa.s^n, $n = 0.6$).

Therefore, according to the results of the performed validations, it can be claimed that in this research the simulation was done correctly and the results obtained were confirmed and validated with the data available in the literature and the source of deviations can be due to model limitations, errors in model parameters, or errors in simulation algorithms or model limitations. It should also be mentioned that in future works, the validation of these results with the Mock blood circulation ring tester and stents made with 3D printing will be fully performed and reported.

3.2 | Results of flow models without stent effect

In this research, after performing the simulation on all the proposed models for the simulation of blood properties, the values of velocity, and wall shear stress in the flow were obtained and compared for all the models, and all studied models converged. The results of velocity for the blood flow model without the stent, for all Newtonian and non-Newtonian blood flow models, are shown in Figures 6 and 7. Figure 6 depicts the velocity contour in one plane YZ, and Figure 7 demonstrates the velocity graph in different sections (Z = 0, 0.00575, 0.0115, 0.01725, 0.023 m).

The graph in Figure 7 shows the velocity profile up to the time of development, and as it can be seen, the further the flow gets closer to the developed flow, the less the difference between the velocity graphs. For models of blood flow in the assumed symmetric vessel, the results of velocity profiles were observed to be symmetric and parabolic.

As found in the results, the difference between Newtonian and non-Newtonian models was evident. In addition, a similarity between the Newtonian and non-Newtonian power-law models was observed in the results, which was due to the selection of the parameters of the non-Newtonian power-law model. As seen in Equation (9) and Table 2, the maximum value of viscosity in the non-Newtonian power-law model is equal to the viscosity of the Newtonian model, which indicates that it is not allowed to advance more than that value. The shape of velocity profiles for different flow models in a smooth vessel can be compared with References 45, 53 and 55–58.

In this section, the contours of pressure and pressure drop along the flow are shown and discussed. Figure 8 depicts the flow pressure contours for all three Newtonian and non-Newtonian models.

In the pressure contours, as shown, the difference between Newtonian and non-Newtonian models was evident. In addition, a similarity between Newtonian and non-Newtonian power-law models was observed in the results, which
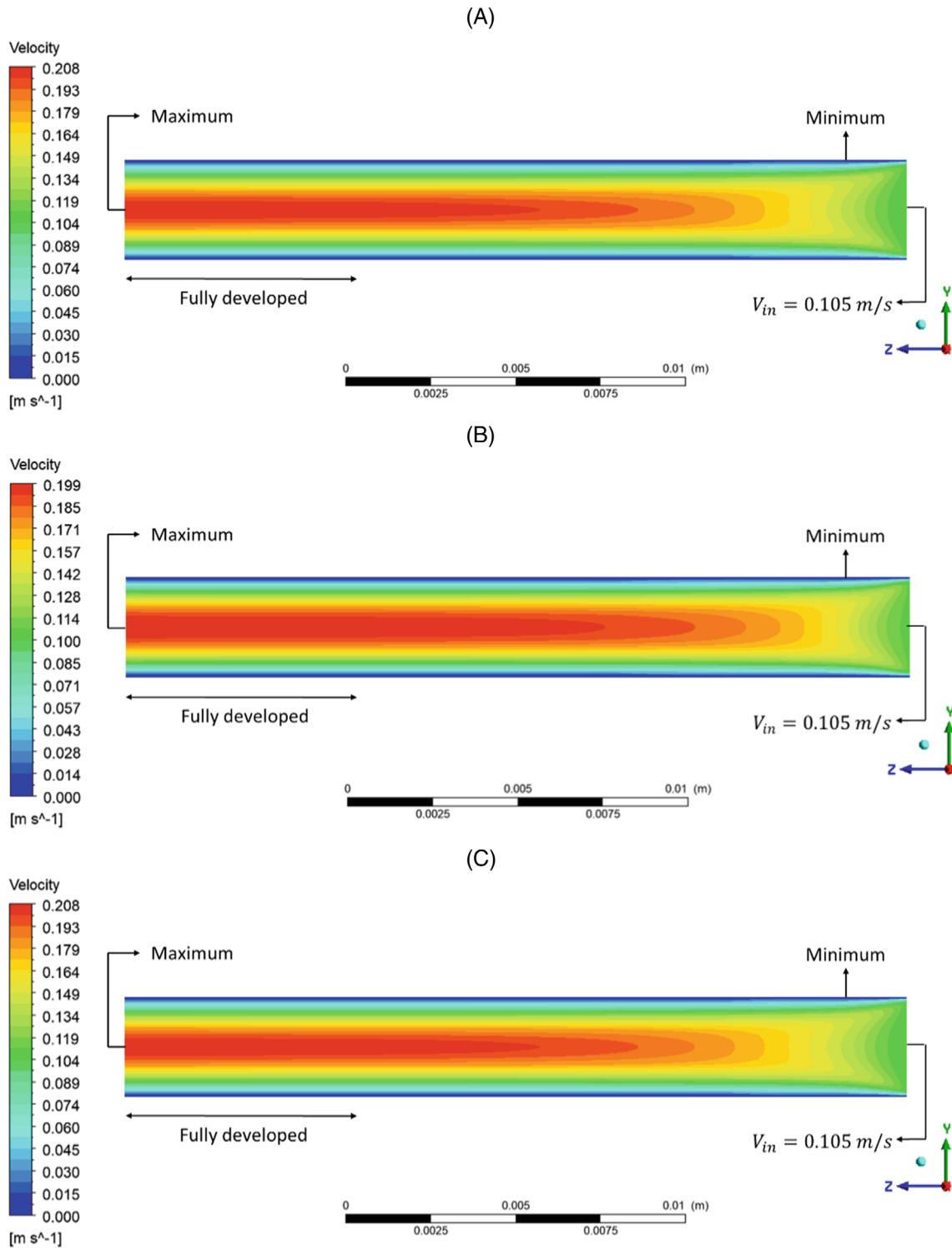
FIGURE 6 Velocity profiles for blood flow by (A) Newtonian, (B) Carreau, and (C) non-Newtonian power-law models.
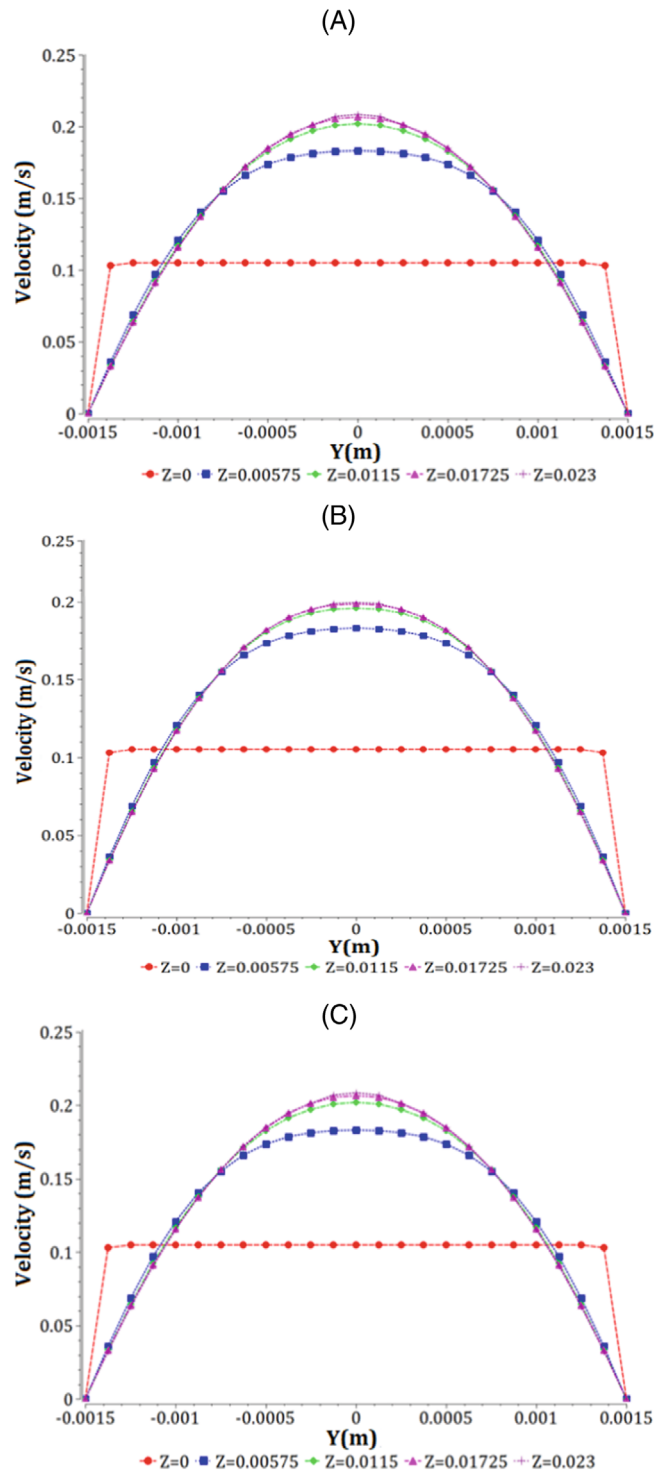
FIGURE 7 Velocity profiles in the different lines (Lines Z = 0, 0.00575, 0.0115, 0.01725, 0.023 m) for blood flow. (A) Newtonian, (B) Carreau, and (C) non-Newtonian power-law models.
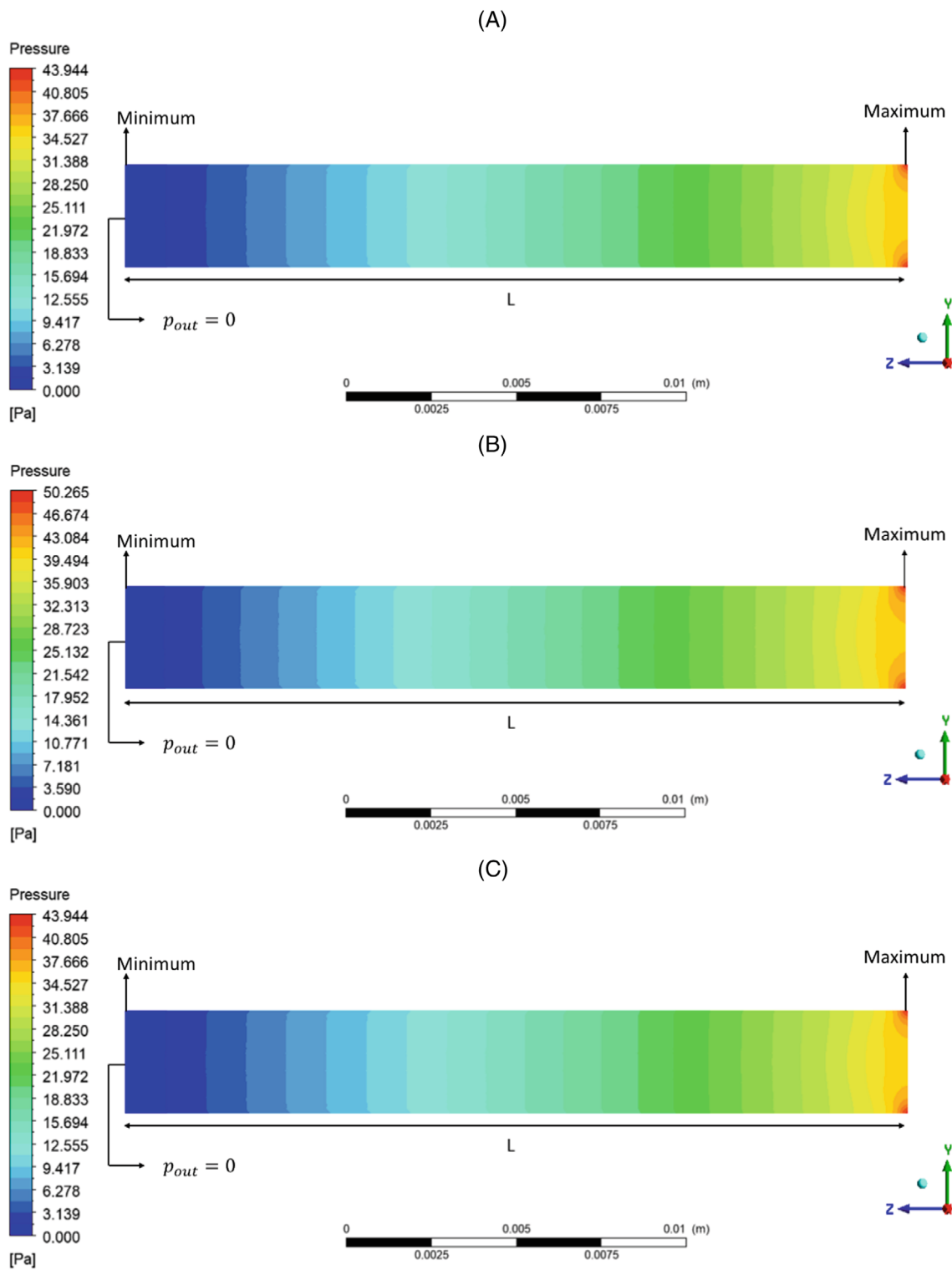
FIGURE 8 Pressure profiles for blood flow by (A) Newtonian, (B) Carreau, and (C) non-Newtonian power-law.

TABLE 5 The pressure drop per unit length for the blood flow without stent effect.

Models	Newtonian	Non-Newtonian	
		Carreau	Power-law
$\frac{\Delta p}{L}\left(\frac{mmHg}{mm}\right)$	0.014	0.016	0.014

was caused by the choice of non-Newtonian power-law model parameters. Moreover, its reasons were investigated and identified in the velocity section. Table 5 demonstrates the pressure drop per unit length of the flow for all three simulated blood flow models.

As it is clear from Table 5, the pressure drop during the flow for the non-Newtonian Carreau fluid was 14.38% higher than the rest of the models. Moreover, the pressure drops for the Newtonian and non-Newtonian power-law flow according to the parameters specified in this article for the flow in a vessel were equal to Newtonian flow.

Figure 9, which shows the wall shear stress distribution contour, shows the minimum and maximum wall shear stress in three different models.

The results in the wall shear stress for a flow in a smooth vessel without a stent, similar velocity, and pressure were equal for two Newtonian and non-Newtonian power-law flow models and were maximum for the Carreau model. To compare the results of the models with each other, Figure 10 depicts a comparison between the results of the models for velocity, pressure drop per unit length, and wall shear stress side by side. Figure 10 compares the results of the models with each other, the comparison between the results of the models for the velocity, pressure drop per unit length, and wall shear stress are illustrated side by side. As can be seen, the behavior of two Newtonian and non-Newtonian power-law models was similar, of course, this issue was according to the defined relationships to determine the range of the non-Newtonian power-law model (Considering the Maximum viscosity limit in the non-Newtonian power-law model is equal to the viscosity of the Newtonian model in Table 2), which was similar to the Newtonian model in this article and has been selected for review and comparison. However, concerning the comparison of the Newtonian model with Carreau, as shown, the maximum velocity in the Carreau model was lower than the Newtonian model due to the same boundary conditions. Moreover, according to the existing relationships, its pressure drop during the flow was higher than in the Newtonian model. In the third part of Figure 10, it can be seen that the wall shear stress in the Carreau model was also higher than in the Newtonian model. These cases can be checked and confirmed according to the equations mentioned in the text, as well as Appendix B.

As it is clear from the results, the distribution of velocity and wall shear stress profiles in blood flow without stents was similar for two Newtonian and non-Newtonian power-law models, although it should be noted that the power-law index affected the behavior of blood flow, so with the parameters determined in Table 2, two Newtonian and non-Newtonian power-law models had close and similar behavior in these results. However, in the Carreau model, the velocity was lower, and naturally, the wall shear stress was higher than those in other models. These results were compared and confirmed with the results of References 47 and 52.

3.3 | Results of flow models with stent effect

In this section, all Newtonian and non-Newtonian blood flow models converged considering the studied stent effect. It should be noted that in this section the stent was placed after the entrance length in the fully developed area discussed in Section 2.1. The results of velocity, pressure, and wall shear stress for the blood flow model considering the stent, for all blood flow models are shown and discussed respectively.

Figures 11 and 12 depict the results of the velocity distribution in the flow with the stent for three blood flow models. Figure 11 demonstrates the velocity contour in one plane YZ, and Figure 12 shows the velocity graph in different sections (Z = 0, 0.00575, 0.0115, 0.01725, 0.023 m). For blood flow models in symmetric vessels, as seen in the graphs of Figure 12, the velocity profiles are symmetric and parabolic.

As can be seen from the velocity distribution in the profiles and graphs in Figures 11 and 12, the velocity at the walls was zero based on the no-slip condition and the inlet velocity was 0.105 m/s. In Figure 12, the velocity profiles at different
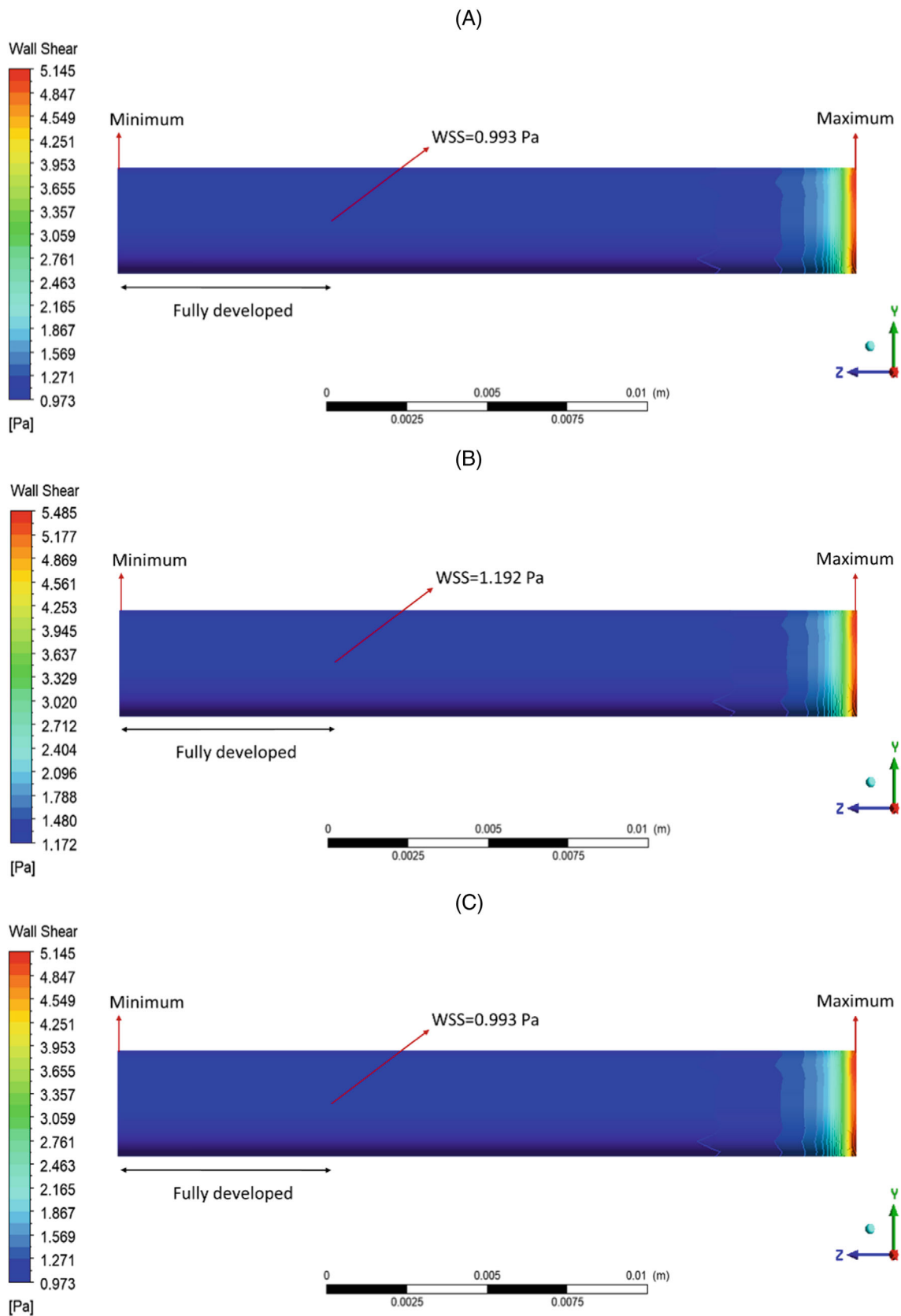
FIGURE 9 Wall shear stress profiles for blood flow by (A) Newtonian, (B) Carreau, and (C) non-Newtonian power-law models.
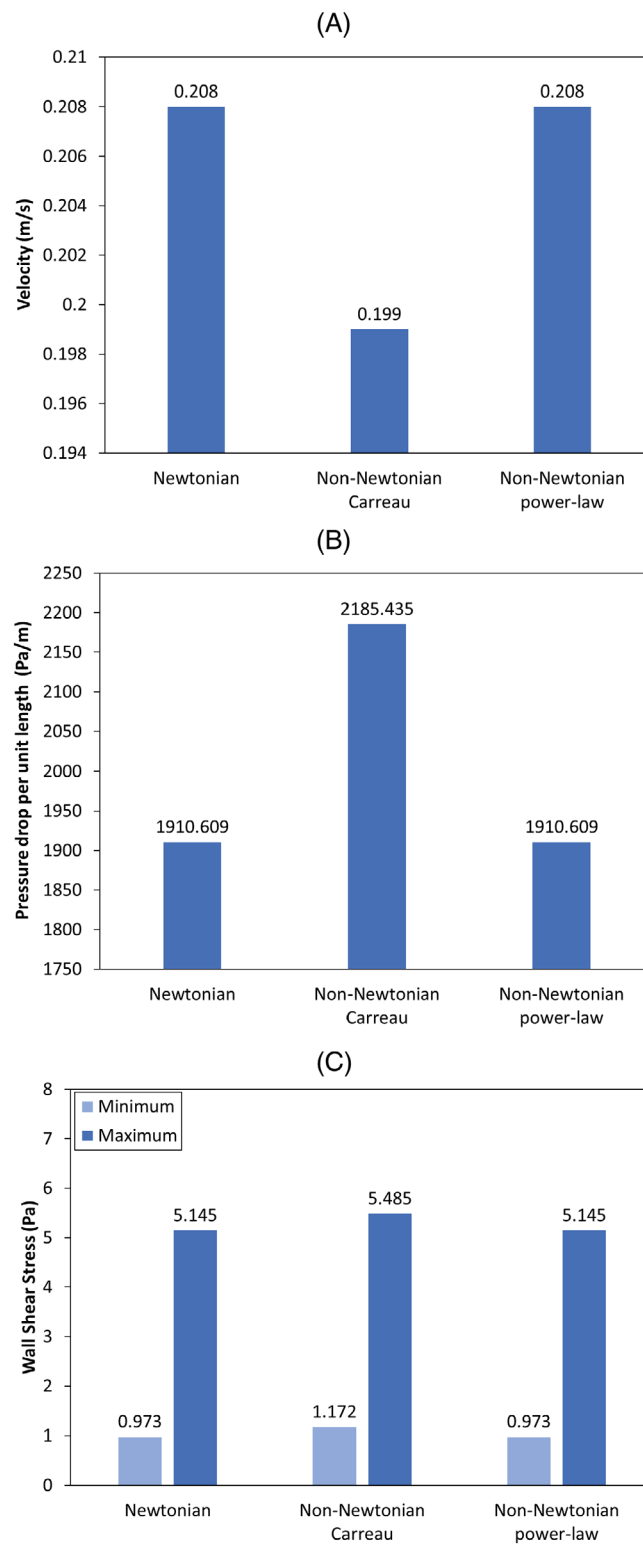
FIGURE 10 The comparison of numerical results in all blood flow models without stent: (A) maximum velocity, (B) pressure drop per unit length, and (C) wall shear stress.
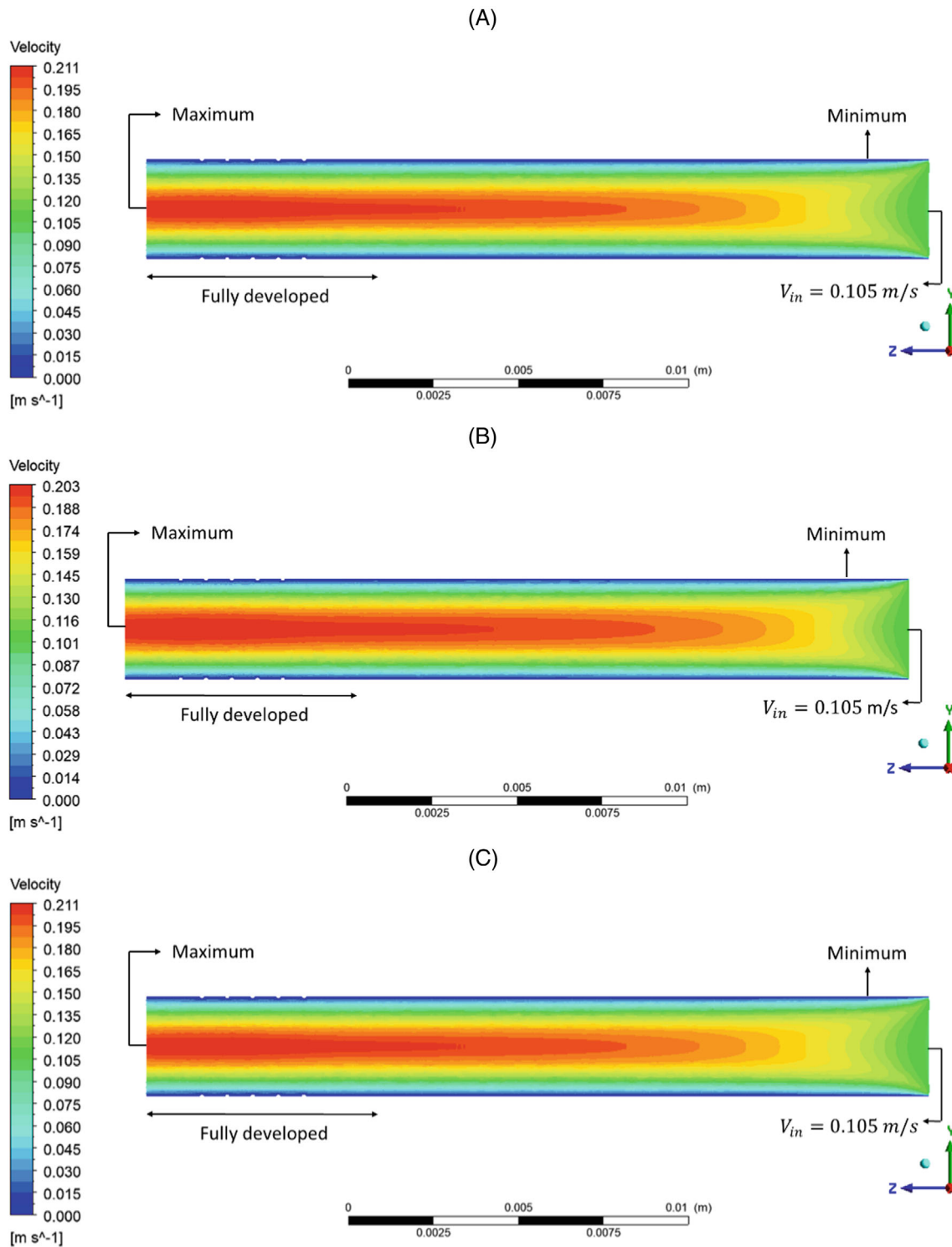
FIGURE 11   Velocity profiles for blood flow with stent effect by (A) Newtonian, (B) Carreau, and (C) non-Newtonian power-law models.
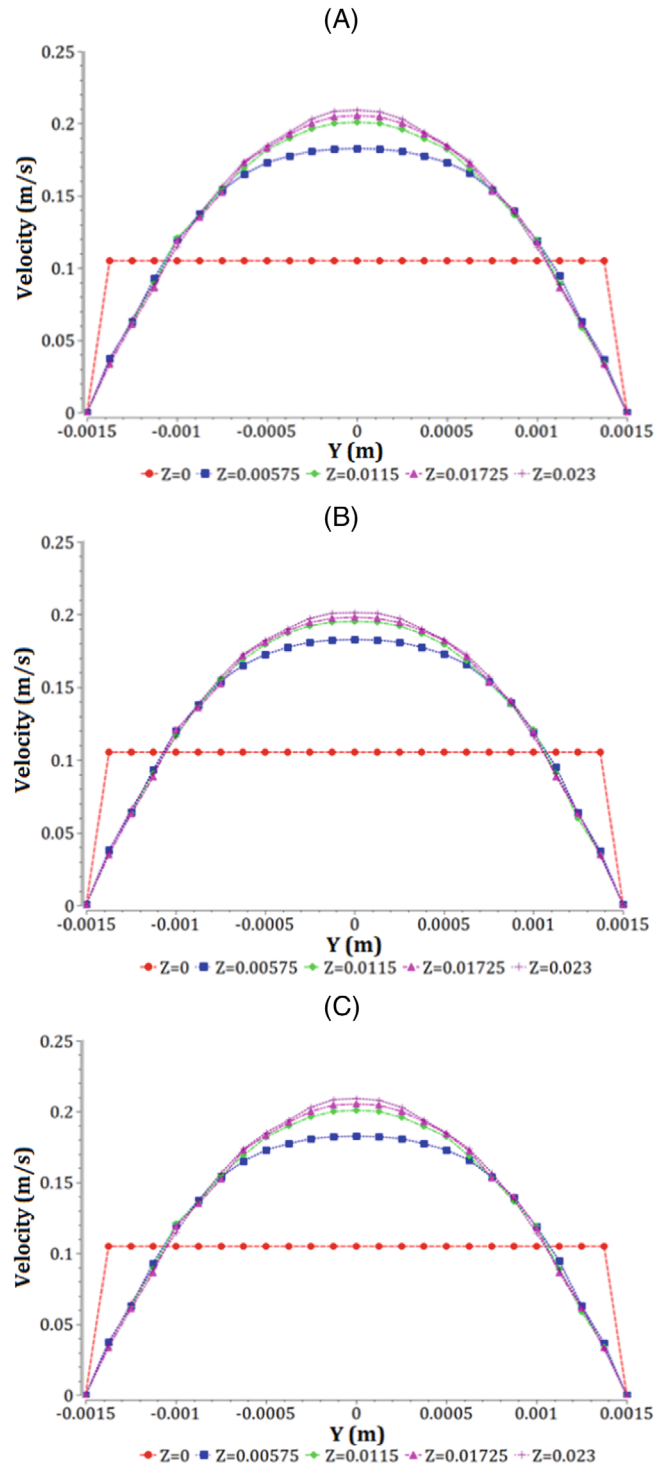
FIGURE 12 Velocity profiles in the different lines (Lines $Z = 0$, 0.00575, 0.0115, 0.01725, and 0.023 m) for blood flow with stent effect by (A) Newtonian, (B) Carreau, and (C) non-Newtonian power-law models.

sections of the flow (Z = 0, 0.00575, 0.0115, 0.01725, 0.023 m) before and after the flow was developed, are drawn, which are clearly defined.

The difference between Newtonian and non-Newtonian models was evident. In addition, a similarity between the Newtonian and non-Newtonian power-law models can be seen in the results, which was due to the parameters selected in Table 2, and also the equality of the maximum viscosity of the non-Newtonian power-law model with the viscosity of the Newtonian model. This similarity and conditions were also confirmed by the reference.[47] The shape of the velocity profiles for different flow models in a smooth vessel can be compared with References 45, 53, 55, 56 and 58.

Figure 13 shows the pressure contours for all three models of blood flow in flow, taking into account the effect of the stent. Table 6 depicts the pressure drop along the flow for all three models of blood flow in flow, taking into account the effect of the stent.

As it is clear from Table 6, the pressure drop during flow for non-Newtonian Carreau fluid was 11.25% higher than that in other models. Then, the pressure drop for flow with a stent was 2.24% higher for Newtonian flow than non-Newtonian power-law.

The wall shear stress distribution during computational fluid dynamics simulation for blood flow with the stent in all models is shown in Figure 14.

The results and references illustrated that the blood flows converge before entering each repeat stent unit and diverge after entering each unit. This divergence reduced the wall shear stress in the vicinity of the stent struts, while on the struts themselves, it was facing an increase in the wall shear stress. In addition, the results indicated that the wall shear stress increased again in the center of each repeated stent unit. This issue was also shown in References 46, 59. Moreover, as can be seen from the results, the wall shear stress for the blood flow with the effect of the stent was also maximum for the Carreau model, which was consistent with the reference.[47]

To compare the results of the models in the flow with the application of the stent effect, a comparison between the results of the models for the velocity, pressure drop per unit length, and wall shear stress is depicted in Figure 15, side by side. As seen in Figure 15, unlike the model without taking into account the stent which the behavior of the Newtonian and non-Newtonian power-law was the same due to considering the maximum viscosity limit of the non-Newtonian power-law model with the viscosity of the Newtonian model, these two models showed a little behavioral difference after considering the stent effect.

As it is clear from the results, the distribution of the velocity profiles in the blood flow with the effect of the stent was similar for Newtonian and non-Newtonian power-law models, and the velocity in the Carreau model was lower than the other two models, and for the wall shear stress results, it can be noted that the shear stress was the highest in the Carreau model, followed by the Newtonian model and then the non-Newtonian power-law model, which results were consistent with References 47 and 52.

3.4 | Comparing results

In Table 7 and Figure 16, the velocity, pressure, and wall shear stress for three blood flow models, Newtonian and Carreau, and non-Newtonian power-law are compared side by side with and without considering the stent effect. Figure 16 shows the results of Table 7 for all three blood flow models for the distribution of maximum velocity, pressure drop per unit length, and wall shear stress, graphically, for flow with and without stent effect.

In the results of the geometric model with a stent effect compared to the geometric model without a stent effect, it was evident that there was higher velocity and wall shear stress because the stent behaved as a cylindrical obstacle in the flow, this is illustrated in Table 7, which was following References 60 and 61. The highest wall shear stress values in the stented part were related to the area of the stent struts, which was specified for all the simulated models. Therefore, the results showed that the wall shear stress increased at the location of the stent struts. This issue was also demonstrated in the studies of References 46 and 59.

In further investigations, the fluid–solid interaction will be reported for such a topic, as also done by the literature[62] for similar studies on the hemodynamics, arterial tissue remodeling, and initiation risk of intracranial aneurysms.
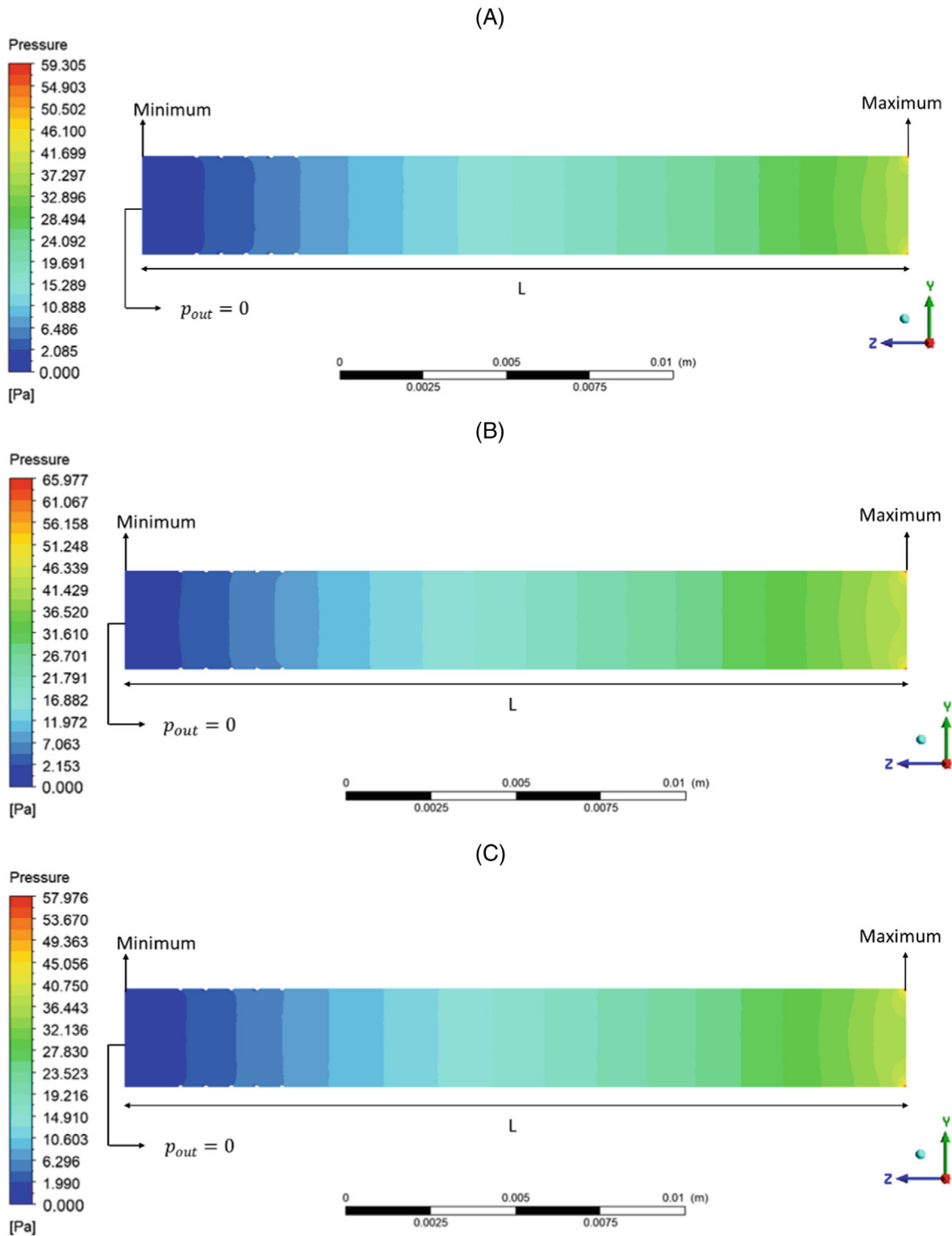
(A)

(B)

(C)

FIGURE 13 Pressure profiles for blood flow with stent effect by (A) Newtonian, (B) Carreau, and (C) non-Newtonian power-law.

TABLE 6 The pressure drop per unit length for blood flow with stent effect.

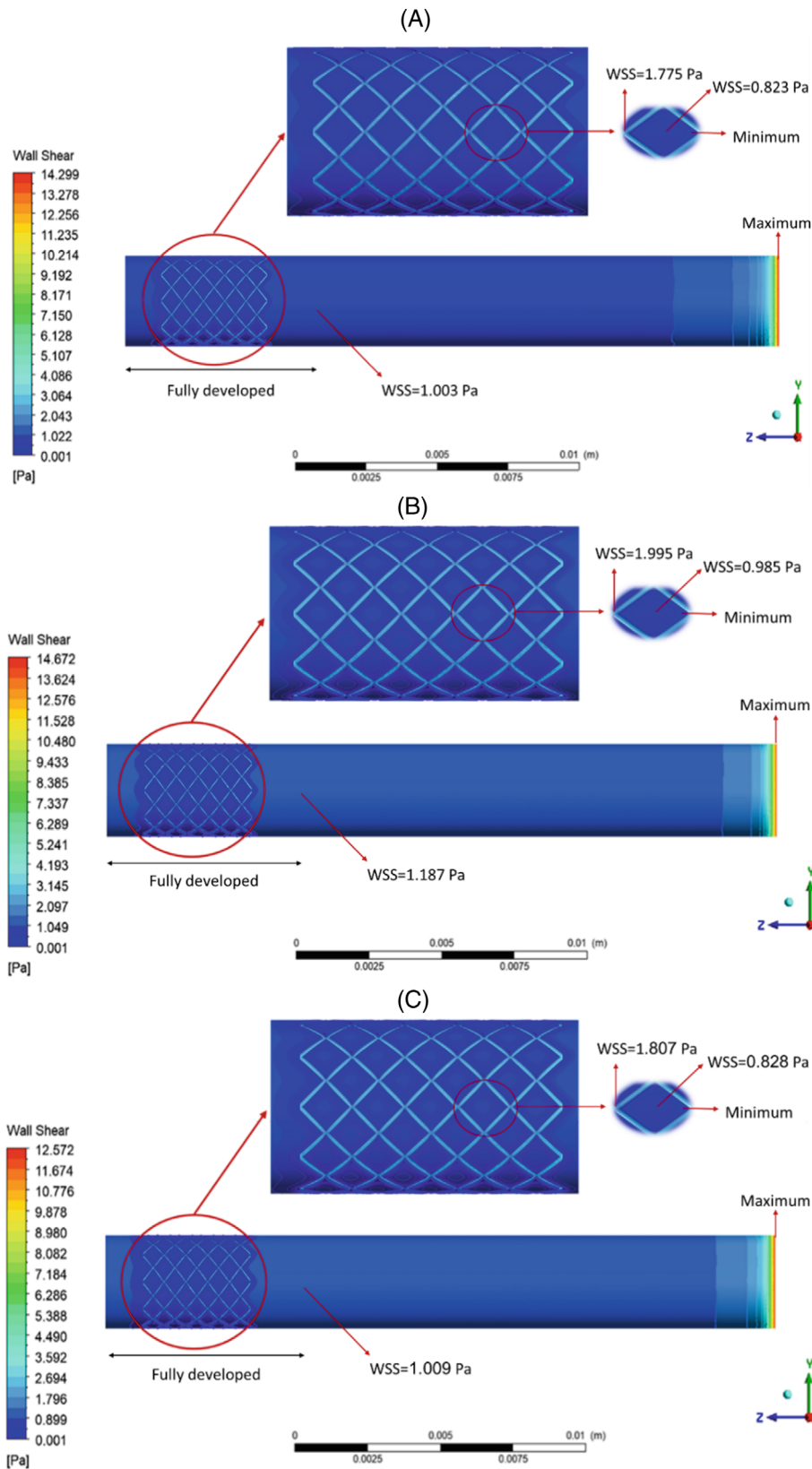|		Non-Newtonian	
Models	**Newtonian**	**Carreau**	**Power-law**
$\frac{\Delta p}{L}\left(\frac{mmHg}{mm}\right)$	0.019	0.021	0.019

FIGURE 14 Wall shear stress profiles for blood flow with stent effect predicted by (A) Newtonian, (B) Carreau, and (C) non-Newtonian power-law models.
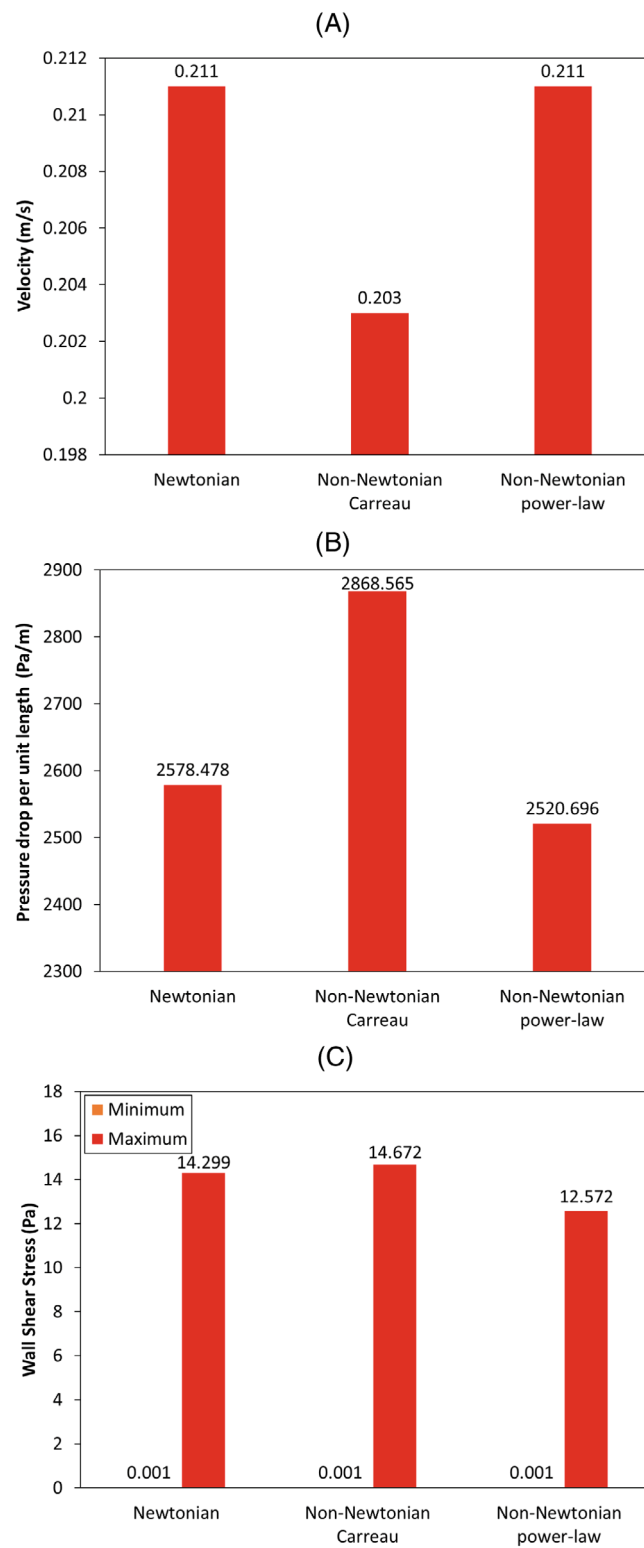
(A)

(B)

(C)

FIGURE 15 The comparison of numerical results in all blood flow models with stent: (A) maximum velocity, (B) pressure drop per unit length, and (C) wall shear stress.

TABLE 7 The comparison of numerical results in all blood flow models with and without stents.

| | | Newtonian | | Non-Newtonian | | | |
| | | | | Carreau | | Power-law | |
Models		Minimum	Maximum	Minimum	Maximum	Minimum	Maximum
Velocity (m/s)	Without stent	0.000	0.208	0.000	0.199	0.000	0.208
	With stent	0.000	0.211	0.000	0.203	0.000	0.211
Pressure (Pa)	Without stent	0.000	43.944	0.000	50.265	0.000	43.944
	With stent	0.000	59.305	0.000	65.977	0.000	57.976
Wall Shear Stress (Pa)	Without stent	0.973	5.145	1.172	5.485	0.973	5.145
	With stent	0.001	14.299	0.001	14.672	0.001	12.572

4 | CONCLUSIONS

In this study, computational fluid dynamics have been simulated for a coronary artery. In this research, the difference in hemodynamic parameters in models built with Newtonian and non-Newtonian fluid assumptions has been investigated, and the effect of stenting on each of the flow models has also been investigated. The results have shown that non-Newtonian models have a significant effect on blood flow dynamics.

The conclusion on the obtained results can be summarized as follows,

1. The distribution of the velocity, pressure, and wall shear stress profiles in blood flow without stents for two Newtonian and non-Newtonian power-law models with the index considered in the article was similar, but in the Carreau model, the velocity was 4.52% lower, the pressure was 12.58% higher, the minimum wall shear stress was 16.98% and the maximum wall shear stress was 6.2% higher than the other two models.
2. The distribution of the velocity profiles in blood flow with stent effect was similar for two Newtonian and non-Newtonian power-law models, and the maximum velocity in the Carreau model was 3.94% lower than the other two models. For the results of pressure in blood flow with the stent effect, it can be noted that the Carreau model illustrated the highest pressure, which was 10.11% more than the Newtonian model, and the non-Newtonian power-law model depicted the lowest pressure, which was 2.29% less than the Newtonian model. For the results of wall shear stress in blood flow with stent effect, it can be noted that the Carreau model indicated the highest shear stress, which was 2.54% more than the Newtonian model, and the non-Newtonian power-law model showed the lowest wall shear stress, which was 13.74% less than the Newtonian model.
3. The highest values of the wall shear stress in the stented part were related to the area of the stent struts. Moreover, the wall shear stress for the blood flow with the effect of the stent was also maximum for the Carreau model.
4. In the results of the geometric model with a stent effect compared to the geometric model without the stent effect, a higher velocity and wall shear stress occurred since the stent behaved as a cylindrical obstacle to the flow.

In further investigations, blood characteristics including the time dependency of properties as well as shear rate dependency of rheological behaviors can be considered in numerical simulations, in addition to elastic, viscoelastic, and hyper-elastic behaviors of arteries. Moreover, according to the specific coronary artery geometry of each patient, research can be personalized from a physiologically realistic point of view for each patient, especially since this issue has a significant impact during stenting and the choice of stent geometry. Finally, a complete validation of numerical results will appear in the next work using the Mock blood circulation ring tester and stents made with 3D printing.
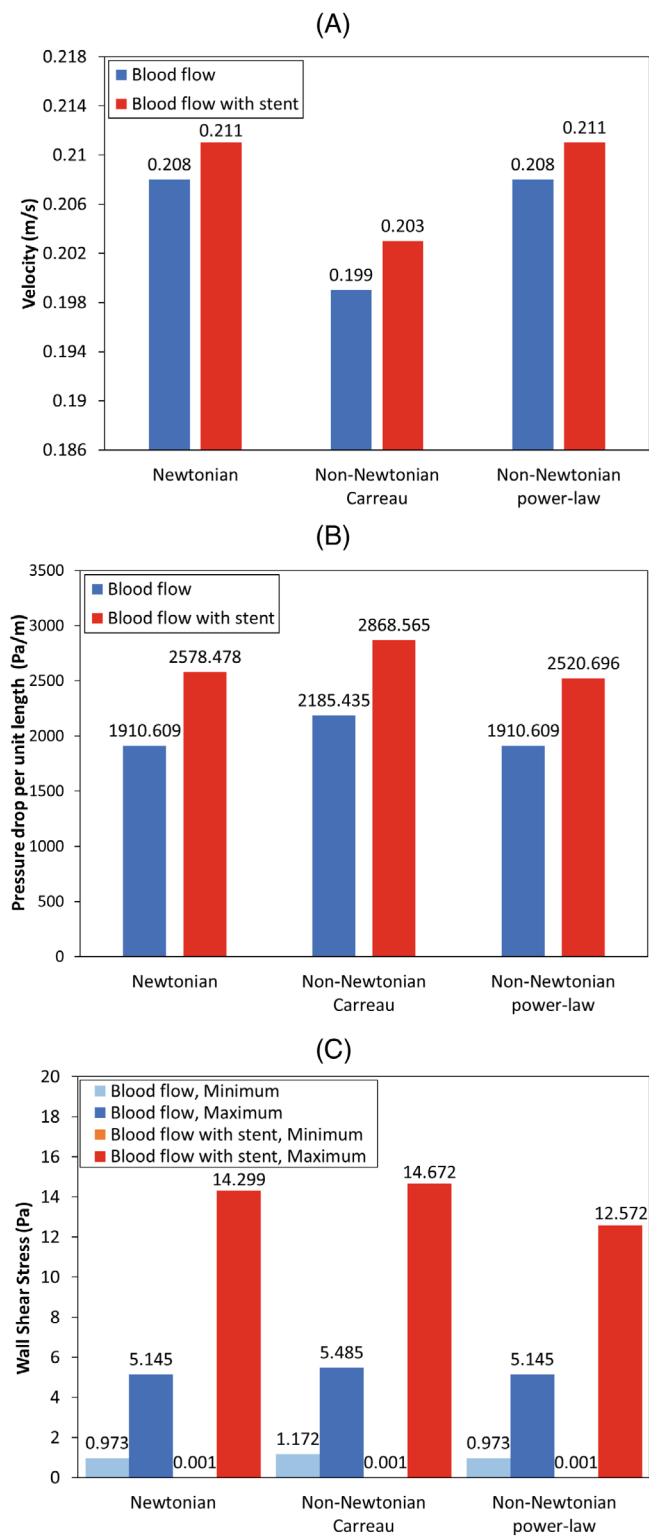
FIGURE 16 The comparison of numerical results in all blood flow models with and without stent: (A) maximum velocity, (B) pressure drop per unit length, and (C) wall shear stress.

NOMENCLATURE

D	Diameter (m)
K	Time constant (s)
k	Consistency Index (kg.s^{n-2}/m)
L	Length (m)
L_e	Entrance length (m)
n	Index
p_{out}	Outlet pressure (Pa)
Re	Reynolds number
T	Temperature (K)
T_0	Reference temperature (K)
V	Velocity (m/s)
V_{in}	Inlet velocity (m/s)
WSS	Wall shear stress (Pa)
$\dot{\gamma}$	Shear rate (1/s)
Δp	Pressure drop (Pa)
μ	Viscosity (kg/m.s)
μ_0	Zero shear viscosity (kg/m.s)
μ_∞	Infinite shear viscosity (kg/m.s)
μ_{min}	Minimum viscosity limit (kg/m.s)
μ_{max}	Maximum viscosity limit (kg/m.s)
ρ	Density (kg/m^3)
τ	Shear stress (Pa)

AUTHOR CONTRIBUTIONS

Fatemeh Ahadi: Data curation (equal); formal analysis (equal); investigation (equal); methodology (equal); software (equal); visualization (equal); writing – original draft (equal). **Mojtaba Biglari:** Conceptualization (equal); investigation (equal); project administration (equal); supervision (equal). **Mohammad Azadi:** Conceptualization (equal); funding acquisition (equal); investigation (equal); methodology (equal); project administration (equal); supervision (equal); validation (equal); writing – review and editing (equal). **Mahdi Bodaghi:** Conceptualization (equal); investigation (equal); project administration (equal); supervision (equal); validation (equal).

FUNDING INFORMATION

CONFLICT OF INTEREST STATEMENT

There is no conflict of interest for all authors.

PEER REVIEW

The peer review history for this article is available at https://www.webofscience.com/api/gateway/wos/peer-review/10.1002/eng2.12779.

DATA AVAILABILITY STATEMENT

All data were presented in the text.

ETHICS STATEMENT

This part is not required for this research.

ORCID

Mohammad Azadi https://orcid.org/0000-0001-8686-8705
Mahdi Bodaghi https://orcid.org/0000-0002-0707-944X

REFERENCES

1. Deplano V, Bailly L, Bertrand E. Influence of blood shear-thinning behavior on flow dynamics in abdominal aortic aneurysm *in vitro* compliant model. *Comput Methods Biomech Biomed Engine*. 2012;15(1):49-52.
2. Taylor CA, Hughes TJR, Zarins CK. Finite element modeling of blood flow in arteries. *Comput Methods Appl Mech Eng*. 1998;158(1–2):155-196.
3. Li G, Chen B, Zhou G. Unsteady non-Newtonian solver on unstructured grid for the simulation of blood flow. *Adv Mech Eng*. 2013;5:596172.
4. Ha YK, Hong H, Yeom E, Song JM. Numerical study of the pulsatile flow depending on non-Newtonian viscosity in a stenosed microchannel. *J Vis*. 2020;23(1):61-70.
5. Chan WY, Ding Y, Tu JY. Modeling of non-Newtonian blood flow through a stenosed artery incorporating fluid-structure interaction. *Aust N Z Ind Appl Math J*. 2007;47:507.
6. Varchanis S, Dimakopoulos Y, Wagner C, Tsamopoulos J. How viscoelastic is human blood plasma? *Soft Matter*. 2018;14:4238-4251.
7. Wootton DM, Ku DN. Fluid mechanics of vascular systems, diseases, and thrombosis. *Annu Rev Biomed Eng*. 1999;1(1):299-329.
8. Liu X, Chen X, Zhang Y, et al. The thermal behavior of blood flow in the arteries with various radii and various stenosis angles using non-Newtonian Sisko model. *Alex Eng J*. 2022;61(9):7195-7201.
9. Caro CG. Vascular fluid dynamics and vascular biology and disease. *Mathematical Methods in the Applied Sciences*. 2001;24(17–18):1311-1324.
10. Huang CR, Pan WD, Chen HQ, Copley AL. Thixotropic properties of whole blood from healthy human subjects. *Biorheology*. 1987;24(6):795-801.
11. Aenis M, Stancampiano AP, Wakhloo AK, Lieber BB. Modeling of flow in a straight stented and nonstented side wall aneurysm model. *J Biomech Eng*. 1997;119(2):206-212.
12. Sohail M, Nazir U, Chu YM, Al-Kouz W, Thounthong P. Bioconvection phenomenon for the boundary layer flow of magnetohydrodynamic Carreau liquid over a heated disk. *Scient Iran*. 2021;28(3):1896-1907.
13. Toghraie D, Esfahani NN, Zarringhalam M, Shirani N, Rostami S. Blood flow analysis inside different arteries using non-Newtonian Sisko model for application in biomedical engineering. *Comput Methods Programs Biomed*. 2020;190:105338.
14. Foong LK, Shirani N, Toghraie D, Zarringhalam M, Afrand M. Numerical simulation of blood flow inside an artery under applying constant heat flux using Newtonian and non-Newtonian approaches for biomedical engineering. *Comput Methods Programs Biomed*. 2020;190:105375.
15. Wu H, Zheng H, Li X, Wang W, Xiang X, Meng X. A geometric accuracy analysis and tolerance robust design approach for a vertical machining center based on the reliability theory. *Measurement*. 2020;161:107809.
16. Deng Z, Wang B, Xu Y, Xu T, Liu C, Zhu Z. Multi-scale convolutional neural network with time-cognition for multi-step short-term load forecasting. *Instit Electr Electron Eng Access*. 2019;7:88058-88071.
17. Deng Z, Liu C, Zhu Z. Inter-hours rolling scheduling of behind-the-meter storage operating systems using electricity price forecasting based on deep convolutional neural network. *Int J Electr Power Energy Syst*. 2021;125:106499.
18. Zajmi L, Ahmed FYH, Jaharadak AA. Concepts, methods, and performances of particle swarm optimization, backpropagation, and neural networks. *Appl Comput Intell Soft Comput*. 2018;2018:1-7.
19. Chen J, Lu XY. Numerical investigation of the non-Newtonian blood flow in a bifurcation model with a non-planar branch. *J Biomech*. 2004;37(12):1899-1911.
20. Perktold K, Peter RO, Resch M, Langs G. Pulsatile non-Newtonian blood flow in three-dimensional carotid bifurcation models: a numerical study of flow phenomena under different bifurcation angles. *J Biomed Eng*. 1991;13(6):507-515.
21. Ku DN, Giddens DP. Pulsatile flow in a model carotid bifurcation. *Arterioscler: Off J Amer Heart Assoc*. 1983;3(1):31-39.
22. Jou LD, Berger SA. Numerical simulation of the flow in the carotid bifurcation. *Theoret Comput Fluid Dyn*. 1998;10(1–4):239-248.
23. Cassar A, Jr DRH, Rihal CS, Gersh BJ, Gps N, Qbujfou F. Chronic coronary artery disease: diagnosis and management. *Mayo Clin Proc*. 2009;84(12):1130-1146.
24. Canfield J, Jain HT. 40 years of percutaneous coronary intervention: history and future directions. *J Pers Med*. 2018;8(4):33.
25. Duhan N, Barak S, Mudgil D. Bioactive lipids: chemistry & health benefits. *Biointerface Res Appl Chem*. 2020;10(6):6676-6687.
26. Darba S, Safaei N, Ahari AM, et al. Direct and indirect costs associated with coronary artery (heart) disease in Tabriz, Iran. *Risk Manag Healthc Policy*. 2020;13:969-978.
27. Iqbal J, Gunn J, Serruys PW. Coronary stents: historical development, current status and future directions. *Br Med Bull*. 2013;106(1):193-211.
28. Grogan JA, Leen SB, Mchugh PE. Comparing coronary stent material performance on a common geometric platform through simulated bench testing. *J Mech Behav Biomed Mater*. 2012;12:129-138.
29. Jiang W, Zhao W, Zhou T, Wang L, Qiu T. A review on manufacturing and post-processing technology of vascular stents. *Micromachines*. 2022;13(1):140.
30. Alam MST, Ansari AQ, Urooj S, Aldobali M. A review based on biodegradable and bioabsorbable stents for coronary artery disease. *Procedia Comput Sci*. 2019;152:354-359.
31. Ahadi F, Azadi M, Biglari M, Bodaghi M, Khaleghian A. Evaluation of coronary stents: a review of types, materials, processing techniques, design, and problems. *Heliyon*. 2023;9:e13575.
32. Andrianov IV, Awrejcewicz J, Diskovsky AA. Structural design of patient-specific vascular ring stents. *Arch Appl Mech*. 2023;93:1473-1490.
33. Etave F, Finet G, Boivin M, Boyer JC, Rioufol G, Thollet G. Mechanical properties of coronary stents determined by using finite element analysis. *J Biomech*. 2001;34(8):1065-1075.

34. Prithipaul PKM, Kokkolaras M, Pasini D. Assessment of structural and hemodynamic performance of vascular stents modelled as periodic lattices. *Med Eng Phys*. 2018;57:11-18.

35. Kolandaivelu K, Swaminathan R, Gibson WJ, et al. Stent thrombogenicity early in high-risk interventional settings is driven by stent design and deployment and protected by polymer-drug coatings. *Circulation*. 2011;123(13):1400-1409.

36. Incropera FP, Dewitt DP, Bergman TL, Lavine AS. *Fundamentals of Heat and Mass Transfer*. 7th ed. Wiley; 2011.

37. Raut BK, Patil VN, Cherian G. Coronary artery dimensions in normal Indians. *Indian Heart J*. 2017;69(4):512-514.

38. Zhou FF, Liu YH, Ge PC, et al. Coronary artery diameter is inversely associated with the severity of coronary lesions in patients undergoing coronary angiography. *Cell Physiol Biochem*. 2017;43(3):1247-1257.

39. Dodge JT, Brown BG, Bolson EL, Dodge HT. Lumen diameter of normal human coronary arteries. Influence of age, sex, anatomic variation, and left ventricular hypertrophy or dilation. *Circulation*. 1992;86(1):232-246.

40. Kahraman H, Ozaydin M, Varol E, et al. The diameters of the aorta and its major branches in patients with isolated coronary artery ectasia. *Tex Heart Inst J*. 2006;33(4):463-468.

41. Goel PK, Vora PL, Sahu AK, Khanna R. Left main coronary artery diameter – a correlation between intravascular ultrasound and quantitative coronary angiography. *Indian Heart J*. 2021;73(5):660-663.

42. Waller BF, Orr CM, Slack JD, Pinkerton CA, Tassel JV, Peters T. Anatomy, histology, and pathology of coronary arteries: a review relevant to new interventional and imaging techniques-part I. *Clin Cardiol*. 1992;15(6):451-457.

43. Kumar A, Lal Ajmani M, Klinkhachorn PS. Morphological variation and dimensions of left coronary artery: a cadaveric study. *MOJ Anat Physiol*. 2018;5(4):266-270.

44. Sahni IJD. Origin and size of the coronary arteries in the north-west Indians. *Indian Heart*. 1989;41(4):221-228.

45. Mohammed AM, Ariane M, Alexiadis A. Fluid-structure interaction in coronary stents: a discrete multiphysics approach. *Chem Eng*. 2021;5(3):60.

46. LaDisa JF, Olson LE, Hettrick DA, Warltier DC, Kersten JR, Pagel PS. Axial stent strut angle influences wall shear stress after stent implantation: analysis using 3D computational fluid dynamics models of stent foreshortening. *Biomed Eng*. 2005;4(1):59.

47. Eltayeb EM, Seory AMA. Study of an artificial heart: design and simulation. *Research Gate Publication*. 2016, version 1, 297013927.

48. Muniandy BK, Ridzuan PD. *Non-Newtonian Computational Fluid Dynamics (CFD) Modeling on Blood Clot Extraction*. Faculty of Chemical Engineering, University Technology Petronas, Malaysia; 2013.

49. Liu H, Lan L, Abrigo J, et al. Comparison of Newtonian and non-Newtonian fluid models in blood flow simulation in patients with intracranial arterial stenosis. *Frontiers Physiology*. 2021;12:718540.

50. Doost SN, Zhong L, Su B, Morsi YS. The numerical analysis of non-Newtonian blood flow in human patient-specific left ventricle. *Comp Methods Programs Biomed*. 2016;127:232-247.

51. Petkova S, Hossain A, Naser J, Palombo E. CFD Modeling of blood flow in portal vein hypertension with and without thrombosis. Third International Conference on CFD in the Minerals and Process Industries. 2003.

52. Chan WY, Eng B. *Simulation of Arterial Stenosis Incorporating Fluid-Structural Interaction and Non-Newtonian Blood Flow*. Faculty of Engineering, RMIT University, Australia; 2005.

53. Mahrous SA, Sidik NAC, Saqr KM. Investigation of Newtonian and power-law blood flow models in a 180° curved pipe at low to medium shear rate. *J Adv Res Fluid Mech Thermal Sci*. 2020;69(1):148-162.

54. White FM. *Fluid Mechanics*. 7th ed. McGraw-Hill; 2009.

55. Ashrafizaadeh M, Bakhshaei H. A comparison of non-Newtonian models for lattice Boltzmann blood flow simulations. *Comput Math Appl*. 2009;58(5):1045-1054.

56. Sankar DS, Hemalatha K. A non-Newtonian fluid flow model for blood flow through a catheterized artery—steady flow. *App Math Model*. 2007;31(9):1847-1864.

57. Mahrous SA, Sidik NAC, Saqr KM. Newtonian and non-Newtonian CFD models of intracranial aneurysm: a review. *CFD Lett*. 2020;12(1):62-86.

58. Kavitha P. Computational methods for non-Newtonian power law fluids. *J Crit Rev*. 2020;7(13):20-40.

59. La Disa JF Jr, Olson LE, Guler I, et al. Circumferential vascular deformation after stent implantation alters wall shear stress evaluated with time-dependent 3D computational fluid dynamics models. *J Appl Physiol*. 2005;98(3):947-957.

60. Gosling RC, Morris PD, Lawford PV, Hose DR, Gunn JP. Predictive physiological modeling of percutaneous coronary intervention – is virtual treatment planning the future? *Front Physiol*. 2018;9:1107.

61. Mortier P, Wentzel JJ, Santis GD, et al. Patient-specific computer modelling of coronary bifurcation stenting: the John doe programme. *EuroIntervention*. 2015;11:35-39.

62. Alilou AAR, Jarrah HR, Zolfagharian A, Bodaghi M. Fluid–structure interaction (FSI) simulation for studying the impact of atherosclerosis on hemodynamics, arterial issue remodeling, and initiation risk of intracranial aneurysms. *Biomech Model Mechanobiol*. 2022;21:1393-1406.

APPENDIX A

In Table A1, different vessel diameters are given to select the vessel diameter for simulation.

T A B L E A1 Diameters of different types of coronary artery vessels.

Vessel types	Diameter range (mm)	References
Proximal LAD	3.27 ± 0.23	34
Proximal RCA	3.20 ± 0.27	34
The average diameter of coronary artery	2.87 ± 0.37	35
LAD	2.26 ± 0.41	35
RCA	2.95 ± 0.60	35
Proximal LAD	3.70 ± 0.40	36
Proximal RCA	2.8 ± 0.50 to 3.90 ± 0.60	36
LMCA	4.13 ± 0.53	37
LAD (p)	3.43 ± 0.67	37
LAD (m)	3.01 ± 0.52	37
LAD (d)	2.39 ± 0.51	37
RCA (p)	2.93 ± 0.68	37
RCA (m)	2.81 ± 0.70	37
RCA (d)	2.24 ± 0.55	37
Ostio-proximal LAD	3.36 ± 0.28	38
LAD	2.00–5.00	39
LAD	4.21 ± 0.28	40
RCA	Female: 2.80 ± 0.40, Male: 3.20 ± 0.50	41

Abbreviations: d, distal segment; LAD, left anterior descending coronary artery; LMCA, left main coronary artery; m, mid segment; p, proximal segment; RCA, right coronary artery.

APPENDIX B

In this appendix, the exact solution equations for laminar Newtonian flow inside the pipe are given[51];

$$u = u_{max}\left(1 - \frac{r^2}{R^2}\right) \text{ where } u_{max} = \left(-\frac{dp}{dx}\right)\frac{R^2}{4\mu} \text{ and } \left(-\frac{dp}{dx}\right) = \left(\frac{\Delta p + \rho g \Delta z}{L}\right),$$

$$V = \frac{Q}{A} = \frac{u_{max}}{2} = \left(\frac{\Delta p + \rho g \Delta z}{L}\right)\frac{R^2}{8\mu},$$

$$Q = \int u dA = \pi R^2 V = \frac{\pi R^4}{8\mu}\left(\frac{\Delta p + \rho g \Delta z}{L}\right),$$

$$\tau_w = \left|\mu \frac{du}{dr}\right|_{r=R} = \frac{4\mu V}{R} = \frac{8\mu V}{d} = \frac{R}{2}\left(\frac{\Delta p + \rho g \Delta z}{L}\right).$$